A Node-Based Smoothed eXtended Finite Element Method (NS-XFEM) for Fracture Analysis

N. Vu-Bac[1], H. Nguyen-Xuan[2], L. Chen[3], S. Bordas[4], P. Kerfriden[4]
R.N. Simpson[4], G.R. Liu[5] and T. Rabczuk[1]

Abstract: This paper aims to incorporate the node-based smoothed finite element method (NS-FEM) into the extended finite element method (XFEM) to form a novel numerical method (NS-XFEM) for analyzing fracture problems of 2D elasticity. NS-FEM uses the strain smoothing technique over the smoothing domains associated with nodes to compute the system stiffness matrix, which leads to the line integrations using directly the shape function values along the boundaries of the smoothing domains. As a result, we avoid integration of the stress singularity at the crack tip. It is not necessary to divide elements cut by cracks when we replace interior integration by boundary integration, simplifying integration of the discontinuous approximation. The key advantage of the NS-XFEM is that it provides more accurate solutions compared to the XFEM-T3 element. We will show for two numerical examples that the NS-XFEM significantly improves the results in the energy norm and the stress intensity factors. For the examples studied, we obtain super-convergent results.

Keywords: Fracture analysis; numerical method, node-based smoothed finite element method, extended finite element method, stress intensity factor (SIF), convergence rate

[1] Institute of Structural Mechanics, Bauhaus-University Weimar, Marienstr. 15, D-99423 Weimar, Germany

[2] Division of Computational Mechanics, Ton Duc Thang University, Ho Chi Minh City, Vietnam

[3] Center for Advanced Computations in Engineering Science (ACES), Department of Mechanical Engineering, National University of Singapore, 9 Engineering Drive 1, Singapore 117576

[4] School of Engineering, Institute of Theoretical, Applied and Computational Mechanics, Cardiff University, Wales, UK

[5] Aerospace Systems Ohio Eminent Scholar University of Cincinnati, Cincinnati, OH 45221-0070

1 Introduction

The classical finite element method (FEM) is quite burdensome for modeling crack growths because it is required to remesh and align the new mesh to the crack's topology. Several finite element techniques such as GFEM [Melenk and Babuška (1997); Strouboulis, Babuška, and Copps (2000)] and XFEM [Belytschko and Black (1999); Moes, Dolbow, and Belytschko (1999)] have been proposed to overcome those difficulties. More recently, the meshfree method has been successful in modeling static and dynamic fracture in 2-dimensions and 3-dimensions performed in [Rabczuk and Belytschko (2004); Rabczuk and Areias (2006); Rabczuk and Eilb (2006); Rabczuk and Belytschko (2007); Rabczuk and Bordas (2007); Rabczuk and Samaniego (2008)].

For the problems with complex geometries, triangular or tetrahedral elements, are usually preferred. However, FEM and XFEM based on such meshes suffer from some difficulties:

- The XFEM based on triangular elements is too stiff.

- The XFEM requires sub-triangulation for integration increasing complexity.

- The XFEM requires the derivatives of the shape function and requires many Gauss points for integrating the crack tip singularity.

We propose a new method to overcome those difficulties. The method is based on the node-based smoothed finite element method (NS-FEM). Smoothing was first used by [Chen, Wu, Yoon, and You (2000)] to stabilize nodal integration in mesh-free method. By combining this strain smoothing technique with the finite element methods, Liu *et al.* have formulated a family of smoothed FEM models named SFEM [Liu, Nguyen, Dai, and Lam (2007); Nguyen-Thanh, Rabczuk, Nguyen-Xuan, and Bordas (2008)], cell-based SFEM (CS-FEM) [Liu, Dai, and Nguyen (2007); Dai, Liu, and Nguyen (2007a); Nguyen-Xuan, Bordas, and Nguyen-Dang (2008); Bordas and Natarajan (2010); Canh, Nguyen-Xuan, Askes, Rabczuk, and Nguyen-Vinh (2010)], node-based SFEM (NS-FEM) [Liu, Nguyen-Thoi, Nguyen-Xuan, and Lam (2009); Nguyen-Thoi, Vu-Do, Rabczuk, and Nguyen-Xuan (2010); Nguyen-Xuan, Rabczuk, Nguyen-Thanh, Nguyen-Thoi, and Bordas (2010)], edge-based SFEM (ES-FEM) [Liu, Nguyen-Thoi, and Lam (2009)], face-based SFEM (FS-FEM) [Nguyen-Thoi, Liu, Lam, and Zhang (2009), alpha-FEM Nguyen-Thanh, Rabczuk, Nguyen-Xuan, and Bordas (2009, 2010)]. In all of these methods, smoothing strain operations are performed over smoothing domains to compute the system stiffness matrix.

In NS-FEM, the system stiffness matrix is calculated by using strain smoothing technique over the cells associated with nodes. As a result, line integration is used along the edges of the smoothing cells instead of volume integration. Moreover, no mapping is needed in the NS-FEM and only the shape functions themselves need to be computed, not their derivatives. It was also shown that the results are less sensitive for distorted elements.

In this paper, we propose a novel numerical method that exploits this special property of the line integration in the NS-XFEM. The system stiffness matrix is computed directly from the special basis shape functions along the boundaries of the smoothing domains. The combination of the NS-FEM and the XFEM can alleviate some of the following difficulties:

1. Simplify integration of discontinuous functions by transforming domain integration on Gauss points into boundary integration by using the divergence theorem. Consequently, there is no need to integrate the $1/\sqrt{r}$ term.

2. The functions to be integrated remain non-polynomial, and optimized one-dimensional integration techniques for these functions are promising routes to increase the accuracy of XFEM.

3. Insensibility to mesh distortion.

4. No subtriangulation is needed for integration reducing complexity.

5. Inherit robustness and accuracy of the triangular NS-FEM.

The paper is outlined as follows. In the next section, we briefly present the basic equations of the NS-FEM. The methodology for coupling NS-FEM and XFEM will be explained in Section 3. Section 4 confirms the accuracy, efficiency and convergence properties of the present method by benchmark problems taken from linear elastic fracture mechanics. Finally, we end the manuscript with concluding remarks and future work.

2   Brief on the node-based smoothed FEM (NS-FEM)

In NS-FEM, the domain is discretized using elements, as in the FEM. However, instead of using the compatible strains, we utilize the "smoothed" strains over the domain Ω divided into a set of smoothing domains N_s as shown in Figure 1 associated with nodes bounded by Ω_k^s, which satisfy the conditions $\Omega = \bigcup_{k=1}^{N_n} \Omega_k^s$ and $\Omega_i^s \cap \Omega_j^s = \emptyset, \forall i \neq j$, in which N_n is the total number of nodes in the element mesh. In this case, $N_s = N_n$. The node-based smoothing domains are employed to smooth the strain field and calculate the stiffness matrix. For the triangular elements, the

smoothing domains Ω_k^s associated with the node k are formed by connecting sequentially the mid-edge-point to the central points (centroids) of the surrounding triangular elements of the node k, as illustrated in Figure 2.
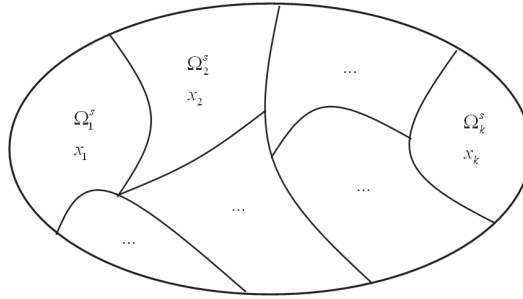
Figure 1: Division of problem domain Ω into non-overlapping smoothing domains Ω_k^s for x_k

Introducing the node-based smoothing operation, the compatible strain $\boldsymbol{\varepsilon} = \nabla_s \mathbf{u}_k^h$ is smoothed over the cell Ω^k associated with node k:

$$\bar{\boldsymbol{\varepsilon}}_k = \int_{\Omega_k^s} \boldsymbol{\varepsilon}(\mathbf{x}) \Phi_k(\mathbf{x}) \, d\Omega = \int_{\Omega_k^s} \nabla_s \mathbf{u}^h(\mathbf{x}) \Phi_k(\mathbf{x}) \, d\Omega \tag{1}$$

where $\Phi_k(\mathbf{x})$ is a given smoothing function that satisfies the following property

$$\int_{\Omega_s^k} \Phi_k(\mathbf{x}) \, d\Omega = 1 \tag{2}$$

Using a constant smoothing function

$$\Phi = \begin{cases} 1/A_k^s & \mathbf{x} \in \Omega_k^s \\ 0 & \mathbf{x} \notin \Omega_k^s \end{cases} \tag{3}$$

It can be shown that

$$\bar{\boldsymbol{\varepsilon}}_k = \frac{1}{A_k^s} \int_{\Omega_k^s} \nabla_s \mathbf{u}^h(\mathbf{x}) \, d\Omega = \frac{1}{A_k^s} \int_{\Gamma_k^s} \mathbf{L}_n \mathbf{u}^h(\mathbf{x}) \, d\Gamma \tag{4}$$
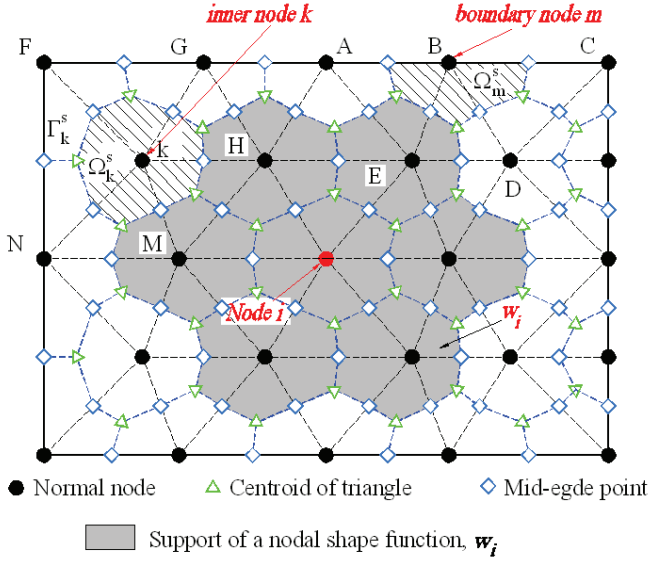
Figure 2: Construction of node-based strain smoothing domains and support domain w_i

where $A_k^s = \int\limits_{\Omega_k^s} d\Omega$ is the area of the smoothing domain Ω_k^s, Γ_k^s is the boundary of the smoothing domain Ω_k^s, and L_n is a matrix comprising of normal components, and is expressed as:

$$
\mathbf{L}_n = \begin{bmatrix} n_x & 0 \\ 0 & n_y \\ n_y & n_x \end{bmatrix} \tag{5}
$$

The discretized strain field $\bar{\boldsymbol{\varepsilon}}_{\mathbf{k}}$ is computed through the so-called smoothed discretized gradient operator or smoothed strain displacement operator, $\bar{\mathbf{B}}$.

$$
\bar{\boldsymbol{\varepsilon}}_k = \sum_{I \in n_k^s} \bar{\mathbf{B}}_I(\mathbf{x}_k) \bar{\mathbf{d}}_I \tag{6}
$$

where $\bar{\mathbf{d}}_{\mathbf{I}}$ are the unknown displacement coefficients defined at the nodes of the finite element, n_k^s is the set of nodes associated to the smoothing domain Ω_k^s. The smoothed element stiffness matrix for element e is computed by the sum of the

contributions of the subcells

$$\bar{\mathbf{K}}_{IJ} = \sum_{k=1}^{N_s} \bar{\mathbf{K}}_{IJ,k}^s = \sum_{k=1}^{N_s} \int_{\Omega_k^s} \bar{\mathbf{B}}_I^{\mathrm{T}} \mathbf{D} \bar{\mathbf{B}}_J \mathrm{d}\Omega = \sum_{k=1}^{N_s} \bar{\mathbf{B}}_I^{\mathrm{T}} \mathbf{D} \bar{\mathbf{B}}_J A_k^s \tag{7}$$

where $\bar{\mathbf{B}}_{\mathbf{I}}(\mathbf{x_k})$ is the smoothed strain gradient matrix:

$$\bar{\mathbf{B}}_I(\mathbf{x}_k) = \begin{bmatrix} \bar{b}_{Ix}(\mathbf{x}_k) & 0 \\ 0 & \bar{b}_{Iy}(\mathbf{x}_k) \\ \bar{b}_{Iy}(\mathbf{x}_k) & \bar{b}_{Ix}(\mathbf{x}_k) \end{bmatrix} \tag{8}$$

with

$$\bar{b}_{Ih}(\mathbf{x}_k) = \frac{1}{A_k^s} \int_{\Gamma_k^s} n_h(\mathbf{x}) N_I(\mathbf{x}) \mathrm{d}\Gamma \; ; \; h = x, y \tag{9}$$

Eq. (9) is now evaluated by line integration along the boundary Γ_k^s of the smoothing domain Ω_k^s. Only the shape function itself is needed to compute the strain displacement matrix leading to simple computations for integration of discontinuous functions in XFEM.

3   Nodal-based smoothed extended finite element method (NS-XFEM)

3.1   *Displacement and Strain Field*

XFEM is based on a local partition of unity. For the case of linear elastic fracture mechanics (LEFM), two sets of enrichment functions are utilized: a Heaviside function to account for the jump across the crack faces and asymptotic branch (near-tip) functions [Belytschko and Black (1999); Rabczuk and Wall (2006)]:

$$\mathbf{u}^h(\mathbf{x}) = \underbrace{\sum_{I \in N^{ns-fem}} N_I(\mathbf{x})\mathbf{d}_I}_{\mathbf{u}^{standard}} + \underbrace{\sum_{J \in N^{ns-c}} N_J(\mathbf{x})H(\mathbf{x})\mathbf{a}_J + \sum_{K \in N^{ns-f}} N_K(\mathbf{x}) \sum_{\alpha=1}^{4} \Phi_\alpha(\mathbf{x})\mathbf{b}_K^\alpha}_{\mathbf{u}^{enr}} \tag{10}$$

where $N_I(\mathbf{x})$, $N_J(\mathbf{x})$ and $N_K(\mathbf{x})$ are finite element shape functions whose support domain is shown in Figure 2, while $\mathbf{d}_I$ are nodal degrees of freedom associated with node I, $\mathbf{a}_J$ and $\mathbf{b}_K$ are additional nodal degrees of freedom corresponding to the Heaviside function $H(\mathbf{x})$ and the near-tip functions, $\{\Phi_\alpha\}_{1 \leqslant \alpha \leqslant 4}$, respectively.

Nodes in set N^{ns-c} are such that their support is split by the crack and nodes in set N^{ns-f} belong to the smoothing domains that contain a crack tip. These nodes

are enriched with the Heaviside and asymptotic branch function fields depicted with squares and circles, respectively, in Figure 5. A set of nodes N^{ns-fem} whose support domain associated with a node of NS-FEM is illustrated in Figure 2.

Now we show how to create the support domain in NS-XFEM. Therefore, we determine the node-based smoothing domains in which at least one $\mathbf{x}$ exists such that $N_I(\mathbf{x}) > 0$, where $N_I(\mathbf{x})$ is the shape function associated with node I. The smoothing domain corresponding to the inner node k, Ω_k^s, is combined from six sub-domains (sub-parts) of elements containing this node. Therefore, the domain Ω_k^s, can be considered to be the smoothing domain of seven nodes from six neighbouring elements: (1) one connectivity node of six neighbouring elements; (2) six remaining points of neighbouring elements. These seven nodes are called the associated nodes of smoothing domain Ω_k^s. The same procedure is applied for the smoothing domain associated with nodes located on the boundary of the domain. The shape of node-based smoothing domains is illustrated in Figure 2 in which FGHMN, ABCDE are associated nodes of smoothing domain Ω_k^s and Ω_m^s, respectively. The support domain of node I is shown by the hatched region in Figure 2.

In NS-XFEM, Heaviside enriched degrees of freedom are added to nodes in N^{ns-c} whose support domain is split by the crack and tip enriched degrees of freedom are added to nodes in set N^{ns-f} whose support domain contains the crack tip. These nodes are depicted by squares and circles, respectively, as shown in Figure 5. According to the chosen nodes, squared nodes are enriched by the step function whereas the circled nodes are enriched by the branch tip functions. In order to keep the convergence rate as high as possible, a so called geometric enrichment should be used that is independent from the discretization [Laborde, Pommier, Renard, and Salaun (2005)]. The $H(\mathbf{x})$ function is given by [Moes, Dolbow, and Belytschko (1999); Rabczuk and Belytschko (2004)].

$$H(\mathbf{x}) = \begin{cases} 1 & (\mathbf{x} - \mathbf{x}^*) \cdot \mathbf{n} \geqslant \mathbf{0} \\ -1 & otherwise \end{cases} \tag{11}$$

where $\mathbf{x}^*$ is a point on the crack surface, see Figure 3

The near tip enrichment consist of functions which incorporate the radial and angular behaviours of the two-dimensional asymptotic crack-tip displacement field [Moes, Dolbow, and Belytschko (1999); Rabczuk and Bordas (2007); Bordas, Rabczuk, Nguyen-Xuan, Nguyen-Vinh, Natarajan, Bog, Do-Minh, and Nguyen-Vinh (2008)]:

$$\{\Phi_\alpha\}_{1\leqslant\alpha\leqslant4} = \sqrt{r}\left\{\sin\left(\frac{\theta}{2}\right),\cos\left(\frac{\theta}{2}\right),\sin(\theta)\sin\left(\frac{\theta}{2}\right),\sin(\theta)\cos\left(\frac{\theta}{2}\right)\right\} \tag{12}$$

where r and θ are polar coordinates in the local crack-tip coordinate system, see Figure 4.
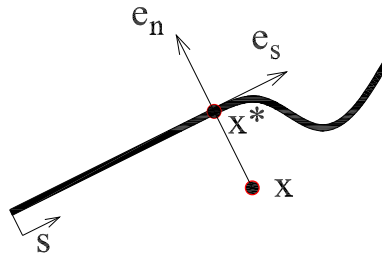
Figure 3: Normal and tangential coordinates for a crack
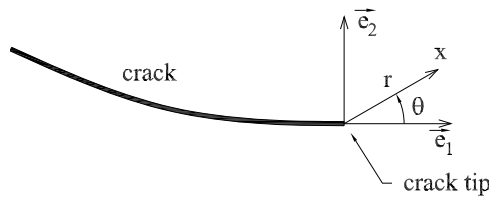
Figure 4: Polar coordinate system associated with a crack tip

In order to keep the enrichment domain narrow, we use a shifting

$$\mathbf{u}^h(\mathbf{x}) = \sum_{I \in N^{ns-fem}} N_I(\mathbf{x})\mathbf{d}_I + \sum_{J \in N^{ns-c}} N_J(\mathbf{x})(H(\mathbf{x}) - H(\mathbf{x}_J))\mathbf{a}_J$$
$$+ \sum_{K \in N^{ns-f}} N_K(\mathbf{x}) \sum_{\alpha=1}^{4} (\Phi_\alpha(\mathbf{x}) - \Phi_\alpha(\mathbf{x}_K))\mathbf{b}_K^\alpha \tag{13}$$

The shifting also circumvents problems due to blending for the Heaviside enrichment but not for the tip enrichment.

Applying the node-based smoothing operation, the smoothed strain associated with node k can be written as:

$$\bar{\boldsymbol{\varepsilon}}_k = \sum_{I \in N_k^s} \bar{\mathbf{B}}_I^u(\mathbf{x}_k)\bar{\mathbf{d}}_I + \sum_{J \in N^{ns-c}} \bar{\mathbf{B}}_J^a(\mathbf{x}_k)(H(\mathbf{x}) - H(\mathbf{x}_J))\mathbf{a}_J$$
$$+ \sum_{k \in N^{ns-f}} \bar{\mathbf{B}}_K^b(\mathbf{x}_k) \sum_{\alpha=1}^{4} (\Phi_\alpha(\mathbf{x}) - \Phi_\alpha(\mathbf{x}_K))\mathbf{b}_K^\alpha \tag{14}$$

where N_k^s is the set of nodes associated with the smoothing domain Ω_k^s, $\bar{\mathbf{B}}_I^{\mathbf{u}}(\mathbf{x}_k)$ is the smoothed strain gradient matrix for the standard NS-FEM part, and $\bar{\mathbf{B}}_I^{\mathbf{a}}(\mathbf{x}_k)$, $\bar{\mathbf{B}}_I^{\mathbf{b}}(\mathbf{x}_k)$ correspond to the enriched parts of the smoothed strain gradient matrix associated with the Heaviside and branch functions, respectively. These matrixes operations can be written as follows:

$$\bar{\mathbf{B}}_I^r(\mathbf{x}_k) = \begin{bmatrix} \bar{b}_{Ix}^r(\mathbf{x}_k) & 0 \\ 0 & \bar{b}_{Iy}^r(\mathbf{x}_k) \\ \bar{b}_{Iy}^r(\mathbf{x}_k) & \bar{b}_{Ix}^r(\mathbf{x}_k) \end{bmatrix} \qquad r = u,\, a,\, b \tag{15}$$

$$\bar{\mathbf{B}}_I^u = \int\limits_{\Gamma_k^s} \frac{1}{A_k^s} \begin{bmatrix} n_x N_I & 0 \\ 0 & n_y N_I \\ n_y N_I & n_x N_I \end{bmatrix} d\Gamma$$

$$\bar{\mathbf{B}}_I^a = \int\limits_{\Gamma_k^s} \frac{1}{A_k^s} \begin{bmatrix} n_x \left[N_I \left(H(\mathbf{x}) - H(\mathbf{x}_I) \right) \right] & 0 \\ 0 & n_y \left[N_I \left(H(\mathbf{x}) - H(\mathbf{x}_I) \right) \right] \\ n_y \left[N_I \left(H(\mathbf{x}) - H(\mathbf{x}_I) \right) \right] & n_x \left[N_I \left(H(\mathbf{x}) - H(\mathbf{x}_I) \right) \right] \end{bmatrix} d\Gamma$$

$$\bar{\mathbf{B}}_I^b = \int\limits_{\Gamma_k^s} \frac{1}{A_k^s} \begin{bmatrix} n_x \left[N_I(\mathbf{x}_{m,n}) \left(\Phi_\alpha(x) - \Phi_\alpha(\mathbf{x}_I) \right) \right] & 0 \\ 0 & n_y [N_I(\mathbf{x}_{m,n}) \left(\Phi_\alpha(\mathbf{x}) - \Phi_\alpha(\mathbf{x}_I) \right)]_{,y} \\ n_y [N_I(\mathbf{x}_{m,n}) \left(\Phi_\alpha(\mathbf{x}) - \Phi_\alpha(\mathbf{x}_I) \right)]_{,y} & n_x [N_I(\mathbf{x}_{m,n}) \left(\Phi_\alpha(\mathbf{x}) - \Phi_\alpha(\mathbf{x}_I) \right)]_{,x} \end{bmatrix} d\Gamma$$
$$(\alpha = 1,\, 2,\, 3 \text{ and } 4) \tag{16}$$

Using Gauss-Legendre integration along Γ_k^s, we obtain:

$$\bar{\mathbf{B}}_I^u = \frac{1}{A_k^s} \begin{bmatrix} \sum\limits_{m=1}^{N_{seg}} \left(\sum\limits_{n=1}^{N_{gau}} n_x(\mathbf{x}_{m,n}) N_I(\mathbf{x}_{m,n}) w_{m,n} \right) & 0 \\ 0 & \sum\limits_{m=1}^{N_{seg}} \left(\sum\limits_{n=1}^{N_{gau}} n_y(\mathbf{x}_{m,n}) N_I(\mathbf{x}_{m,n}) w_{m,n} \right) \\ \sum\limits_{m=1}^{N_{seg}} \left(\sum\limits_{n=1}^{N_{gau}} n_y(\mathbf{x}_{m,n}) N_I(\mathbf{x}_{m,n}) w_{m,n} \right) & \sum\limits_{m=1}^{N_{seg}} \left(\sum\limits_{n=1}^{N_{gau}} n_x(\mathbf{x}_{m,n}) N_I(\mathbf{x}_{m,n}) w_{m,n} \right) \end{bmatrix}$$

$$\bar{\mathbf{B}}_I^a = \frac{1}{A_k^s} \begin{bmatrix} M_1 & 0 \\ 0 & M_2 \\ M_2 & M_1 \end{bmatrix}$$

in which

$$M_1 = \sum_{m=1}^{N_{seg}} \left(\sum_{n=1}^{N_{gau}} \begin{array}{l} n_x(\mathbf{x}_{m,n}) N_I(\mathbf{x}_{m,n}) \times \\ \times \left(H(\mathbf{x}_{m,n}) - H(\mathbf{x}_I) \right) w_{m,n} \end{array} \right)$$

$$M_2 = \sum_{m=1}^{N_{seg}} \left(\sum_{n=1}^{N_{gau}} \begin{array}{l} n_y(\mathbf{x}_{m,n}) N_I(\mathbf{x}_{m,n}) \times \\ \times \left(H(\mathbf{x}_{m,n}) - H(\mathbf{x}_I) \right) w_{m,n} \end{array} \right)$$

$$\bar{\mathbf{B}}_I^b = \frac{1}{A_k^s} \begin{bmatrix} M_3 & 0 \\ 0 & M_4 \\ M_4 & M_3 \end{bmatrix} \tag{17}$$

in which

$$M_3 = \sum_{m=1}^{N_{seg}} \left(\sum_{n=1}^{N_{gau}} \begin{matrix} n_x(\mathbf{x}_{m,n})N_I(\mathbf{x}_{m,n}) \times \\ \times (\Phi_\alpha(bfx_{m,n}) - \Phi_\alpha(\mathbf{x}_I)) \, w_{m,n} \end{matrix} \right)$$

$$M_4 = \sum_{m=1}^{N_{seg}} \left(\sum_{n=1}^{N_{gau}} \begin{matrix} n_y(\mathbf{x}_{m,n})N_I(\mathbf{x}_{m,n}) \times \\ \times (\Phi_\alpha(x) - \Phi_\alpha(\mathbf{x}_I)) \, w_{m,n} \end{matrix} \right)$$

($\alpha = 1, 2, 3$ and 4)

where N_{neg} is the number of segments of the boundary Γ_k^s, N_{gau} is the number of Gauss points used in each segment, $w_{m,n}$ is the corresponding Gauss weights, n_x, n_y are the outward unit normal components to each segment on the smoothing domain boundary and $\mathbf{x}_{m,n}$ is the n-th Gaussian point on the m-th segment of the boundary Γ_k^s.

3.2 *Weak form and discrete equation*

The smoothed Galerkin weak form is given by:

Find $\mathbf{u}^h \in V, \forall \delta\mathbf{u}^h \in V_0$ such that

$$\int_\Omega \delta(\bar{\boldsymbol{\varepsilon}}(\mathbf{u}^h))^{\mathrm{T}} \mathbf{D}(\bar{\boldsymbol{\varepsilon}}(\mathbf{u}^h)) \, \mathrm{d}\Omega - \int_\Omega (\delta\mathbf{u}^h)^{\mathrm{T}} \mathbf{b} \, \mathrm{d}\Omega - \int_\Gamma (\delta\mathbf{u}^h)^{\mathrm{T}} \mathbf{t}_\Gamma \, \mathrm{d}\Gamma = 0 \tag{18}$$

with $V = \{\mathbf{u} \mid \mathbf{u} \in H^1(\Omega \backslash \Gamma_c), \ \mathbf{u} = \bar{\mathbf{u}} \text{ on } \Gamma_u, \ \mathbf{u} \text{ discontinuous on } \Gamma_c\}$
and $V_0 = \{\delta\mathbf{u} \mid \delta\mathbf{u} \in H^1(\Omega \backslash \Gamma_c), \ \delta\mathbf{u} = \mathbf{0} \text{ on } \Gamma_u, \ \delta\mathbf{u} \text{ discontinuous on } \Gamma_c\}$

Substituting the trial and test function into Eq. (18), we finally obtain the well-known equation:

$$\bar{\mathbf{K}}\bar{\mathbf{d}} = \mathbf{f} \tag{19}$$

where $\mathbf{f}$ is the nodal force vector that is identical to that in the standard XFEM. The smoothed enriched stiffness matrix $\bar{\mathbf{K}}$ for all sub-cells is computed by:

$$\bar{\mathbf{K}}_{IJ} = \sum_{k=1}^{N_s} \bar{\mathbf{K}}_{IJ,k}^s$$

$$= \sum_{k=1}^{N_s} \begin{bmatrix} \int\limits_{\Omega_k^s} (\bar{\mathbf{B}}_I^u)^{\mathrm{T}} \mathbf{D}\bar{\mathbf{B}}_J^u \mathrm{d}\Omega & \int\limits_{\Omega_k^s} (\bar{\mathbf{B}}_I^u)^{\mathrm{T}} \mathbf{D}\bar{\mathbf{B}}_J^a \mathrm{d}\Omega & \int\limits_{\Omega_k^s} (\bar{\mathbf{B}}_I^u)^{\mathrm{T}} \mathbf{D}\bar{\mathbf{B}}_J^b \mathrm{d}\Omega \\ \int\limits_{\Omega_k^s} (\bar{\mathbf{B}}_I^a)^{\mathrm{T}} \mathbf{D}\bar{\mathbf{B}}_J^u \mathrm{d}\Omega & \int\limits_{\Omega_k^s} (\bar{\mathbf{B}}_I^a)^{\mathrm{T}} \mathbf{D}\bar{\mathbf{B}}_J^a \mathrm{d}\Omega & \int\limits_{\Omega_k^s} (\bar{\mathbf{B}}_I^a)^{\mathrm{T}} \mathbf{D}\bar{\mathbf{B}}_J^b \mathrm{d}\Omega \\ \int\limits_{\Omega_k^s} (\bar{\mathbf{B}}_I^b)^{\mathrm{T}} \mathbf{D}\bar{\mathbf{B}}_J^u \mathrm{d}\Omega & \int\limits_{\Omega_k^s} (\bar{\mathbf{B}}_I^b)^{\mathrm{T}} \mathbf{D}\bar{\mathbf{B}}_J^a \mathrm{d}\Omega & \int\limits_{\Omega_k^s} (\bar{\mathbf{B}}_I^b)^{\mathrm{T}} \mathbf{D}\bar{\mathbf{B}}_J^b \mathrm{d}\Omega \end{bmatrix} \tag{20}$$

In NS-XFEM, the stiffness matrix in Eq. (20) can therefore be rewritten as:

$$
\bar{\mathbf{K}}_{IJ} = \sum_{k=1}^{N_s} \bar{\mathbf{K}}_{IJ,k}^s = \sum_{k=1}^{N_s}
\begin{bmatrix}
(\bar{\mathbf{B}}_I^u)^{\mathrm{T}} \mathbf{D} \bar{\mathbf{B}}_J^u A_k^s & (\bar{\mathbf{B}}_I^u)^{\mathrm{T}} \mathbf{D} \bar{\mathbf{B}}_J^a A_k^s & (\bar{\mathbf{B}}_I^u)^{\mathrm{T}} \mathbf{D} \bar{\mathbf{B}}_J^b A_k^s \\
(\bar{\mathbf{B}}_I^a)^{\mathrm{T}} \mathbf{D} \bar{\mathbf{B}}_J^u A_k^s & (\bar{\mathbf{B}}_I^a)^{\mathrm{T}} \mathbf{D} \bar{\mathbf{B}}_J^a A_k^s & (\bar{\mathbf{B}}_I^a)^{\mathrm{T}} \mathbf{D} \bar{\mathbf{B}}_J^b A_k^s \\
(\bar{\mathbf{B}}_I^b)^{\mathrm{T}} \mathbf{D} \bar{\mathbf{B}}_J^u A_k^s & (\bar{\mathbf{B}}_I^b)^{\mathrm{T}} \mathbf{D} \bar{\mathbf{B}}_J^a A_k^s & (\bar{\mathbf{B}}_I^b)^{\mathrm{T}} \mathbf{D} \bar{\mathbf{B}}_J^b A_k^s
\end{bmatrix}
\tag{21}
$$

3.3 Numerical integration

3.3.1 Numerical integration for the XFEM.

There are four types of elements used for numerical integration as mentioned in [Bordas, Rabczuk, Nguyen-Xuan, Nguyen-Vinh, Natarajan, Bog, Do-Minh, and Nguyen-Vinh (2008)]:

- *Tip elements* contain the crack tip. All nodes belonging to a tip element are enriched with the branch functions, Eq. (12).

- *Split elements* are elements completely cut by the crack. Their nodes are enriched with the step function, Eq. (11).

- *Tip-blending elements* are elements neighboring tip elements. Some of their nodes are enriched with branch functions, while others are not enriched at all.

- *Split-blending elements* are elements neighboring split elements. Some of their nodes are enriched with the Heaviside function, while others are not enriched.

- *Standard elements* are elements that are in neither of the above categories. None of their nodes are enriched.

Since the approximation differs from element to element, different integration parameters are used. For XFEM built on T3 elements, we chose the following Gauss quadrature rules as [Bordas, Rabczuk, Nguyen-Xuan, Nguyen-Vinh, Natarajan, Bog, Do-Minh, and Nguyen-Vinh (2008)]

1. *Tip elements*: 7 Gauss points for each sub-element.

2. *Split elements*: 1 Gauss points for each sub-element.

3. *Tip-blending elements*: 7 Gauss points.

4. *Split-blending elements*: 1 Gauss point.

5. *Standard elements*: 1 Gauss point.

3.3.2   Numerical integration for the NS-XFEM.

There are five types of smoothing domains (sd) as shown in Figure 5:
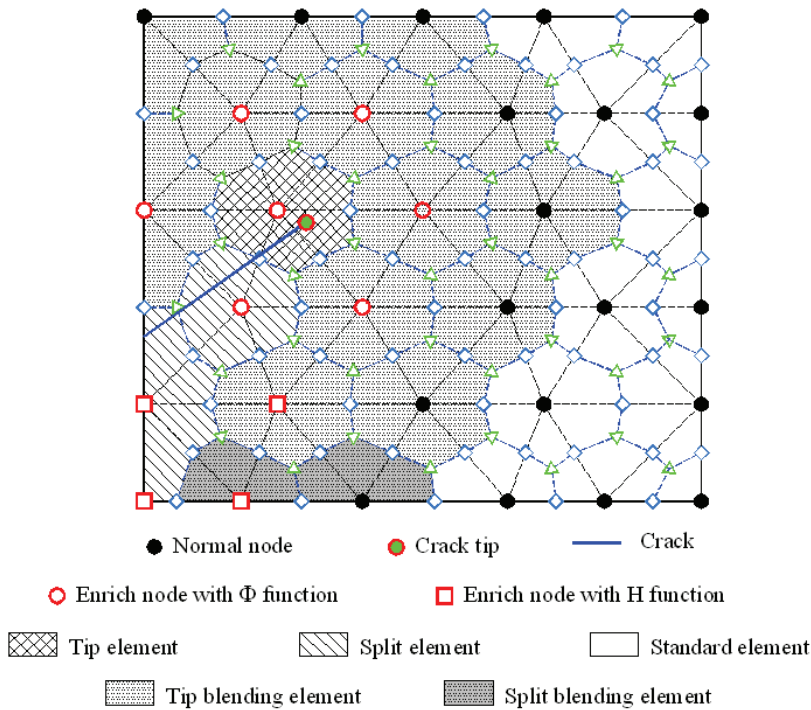
Figure 5: Illustration of node-based smoothing domain (sd) and node categories in NS-XFEM in term of the support domain of nodal shape function

- *Tip smoothing domains* contain a crack tip. All nodes are enriched with branch functions.

- *Split smoothing domains* are completely cut by a crack surface, and their nodes are enriched with the Heaviside function.

- In *Tip-blending smoothing domains*, one or more nodes are enriched with branch functions, and others are not enriched at all.

- *Split-blending smoothing domains* contain step enriched nodes and not enriched nodes

- *Standard smoothing domains* are smoothing domains that are in none of the above categories. None of their nodes are enriched.

(*i*) *Split smoothing domains*: To perform Gauss integration for split smoothing domains, it is inevitable to divide them into several triangles and then use the familiar quadrature rules. However, the complex interior integration can be replaced by boundary integration which can be implemented on polygonal boundaries of sub-domains [Bordas, Rabczuk, Nguyen-Xuan, Nguyen-Vinh, Natarajan, Bog, Do-Minh, and Nguyen-Vinh (2008)]. One Gauss point on each boundary segment for split smoothing domains is sufficient. The scheme of partitioning the split smoothing domain is shown in Figure 6.

(*ii*) *Split-blending smoothing domains*: Partitioning of smoothing domains is not necessary. One Gauss point on each boundary segment is sufficient.

(*iii*) *Tip smoothing domains*: Special care has to be taken. Simply splitting the smoothing domains into sub-domains is not sufficient to guarantee accurate results [Laborde, Pommier, Renard, and Salaun (2005)]. A higher integration density should be used close to crack tip. We propose the following procedure: (1) Splitting the smoothing domain into triangles as shown in Figure 7; (2) Dividing triangle into n_{sc} sub-cells (also triangles) following the rules giving in Figure 8. Figure 7 shows the sub-cells after dividing sub-sd1 and sub-sd3 with $n_{sc} = 3$, e.g., sub-sd1 is split into sc1, sc2 and sc3; and sub-sd3 is split into sc4, sc5 and sc6; (3) The numerical integration is then performed on boundaries of triangular cells.

When we perform boundary integration along the crack face over sub-cells whose boundary segments coincide with the crack surface, so-called c-sub-cells are used as illustrated in Figure 7. For example two c-sub-cells that share a boundary segment along the crack surface 79 are used (sc3 and sc6). Although the values of discontinuous function, $H(\mathbf{x})$, or branch functions, $\Phi_\alpha(\mathbf{x})$ for both c-sub-cells are the same, the displacement between two sides of crack has a jump and it is obviously not compatible with the above calculations. A remedy for this problem is proposed in which we calculate the values of the enrichment $H(\mathbf{x})$ and branch functions, $\Phi_\alpha(\mathbf{x})$ at the center instead of Gauss points on the side of this sub-cell.

Numerical experiments [Chen, Rabczuk, Liu, Zeng, Kerfriden, and Bordas (2010)] suggest that eight smoothing cells in a smoothing domain ($n_{sc} = 8$),

and five Gauss points on a segment of smoothing cells ($n_{sc} = 5$) are sufficient. This rule is also used in this paper.

(*iv*) *Tip-blending smoothing domains*: no partition is required, and we also use eight smoothing cells in a smoothing domain with five Gauss points on each boundary segment.

(*v*) *Standard smoothing domains* are computed as in NS-FEM.
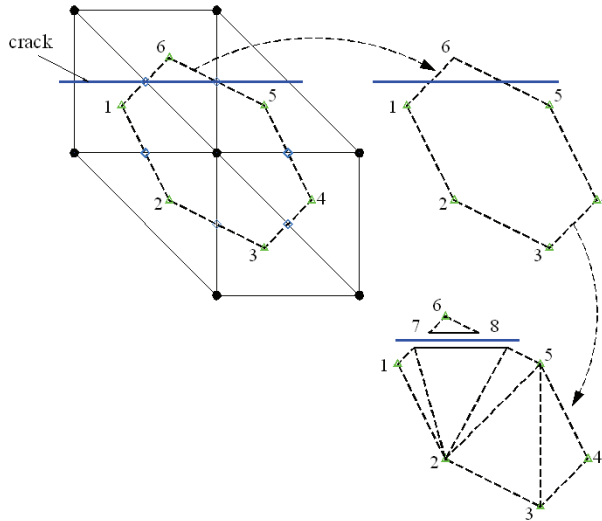
Figure 6: Partitioning split smoothing domain into triangular sub-domains (triangles)

3.4 Stress intensity factor

Fracture parameters such as mode I and mode II stress intensity factors (SIFs) are determined using the domain form [Li, Shih, and Needleman (1985); Moran and Shih (1987)] of the interaction integral [Yau, Wang, and Corten (1980)]. All the finite elements within a radius of $r_d = r_k h_e$ from the crack-tip are selected. Here, h_e is the crack-tip element size and r_k is a scalar.
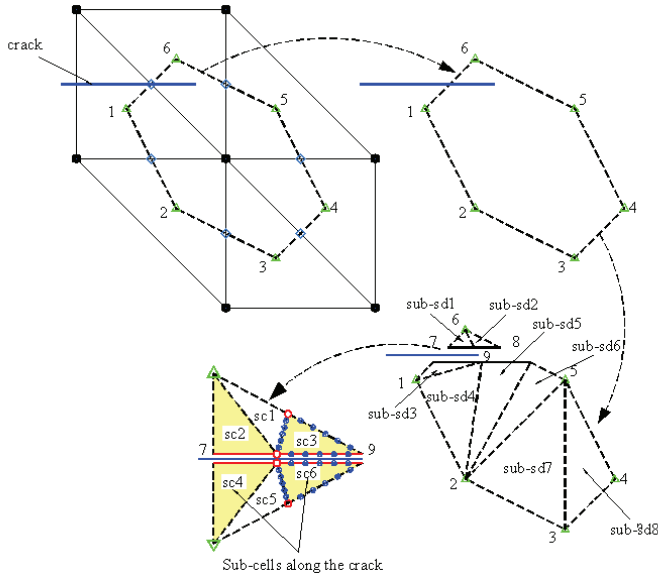
Figure 7: Partitioning tip smoothing domain into triangular sub-domains(triangles)

4 Numerical results

4.1 Plate with edge-crack under tension

Consider a plate under uniaxial tension as shown in Figure 9. Plate's dimension is mm. The material parameters are Young's modulus $E = 3 \times 10^7 Pa$ and Poisson's ratio $v = 0.3$; plane strain conditions are assumed. The reference mode I SIF is given by:

$$K_I^{exact} = F\left(\frac{a}{b}\right)\sigma\sqrt{a\pi} = 1.6118 Pa\sqrt{mm} \tag{22}$$

where $a = 0.3$ is the crack length, b is the plate width and $F\left(\frac{a}{b}\right)$ is given by

$$F\left(\frac{a}{b}\right) = 1.12 - 0.231\left(\frac{a}{b}\right) + 10.55\left(\frac{a}{b}\right)^2 - 21.72\left(\frac{a}{b}\right)^3 + 30.39\left(\frac{a}{b}\right)^4 \tag{23}$$

The strain energy and the error in the energy norm are defined as:

$$E_{(\Omega)} = \frac{1}{2}\int_{\Omega} \boldsymbol{\varepsilon}^T \mathbf{D}\boldsymbol{\varepsilon} d\Omega \tag{24}$$
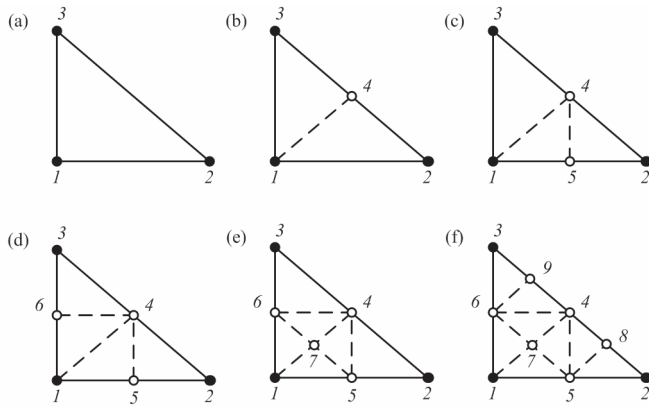
Figure 8: Division of a sub-smoothing domain into sub-smoothing cells (a)n_{sc} = 1; (b)n_{sc} = 2; (c)n_{sc} = 3; (d)n_{sc} = 4; (e)n_{sc} = 6; (f)n_{sc} = 8
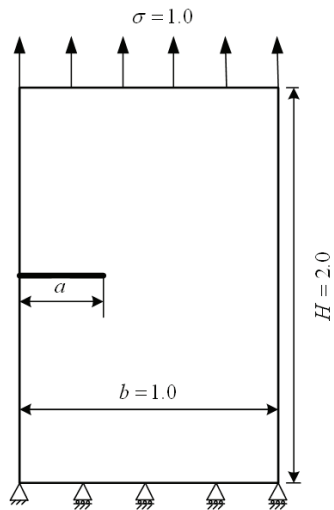
Figure 9: Plate with edge crack under tension

$$e_e = \left| \frac{E^{num}_{(\Omega)} - E^{ref}_{(\Omega)}}{E^{ref}_{(\Omega)}} \right|^{1/2} \tag{25}$$

$$e_k = \left| \frac{K^{num}_{sif} - K^{ref}_{sif}}{K^{ref}_{sif}} \right|^{1/2} \times 100\%, \quad sif = I, II \tag{26}$$

where the superscript "ref" denotes the exact or reference solution, and "num" denotes the numerical solution.

We subsequently consider the following NS-XFEM formulations:
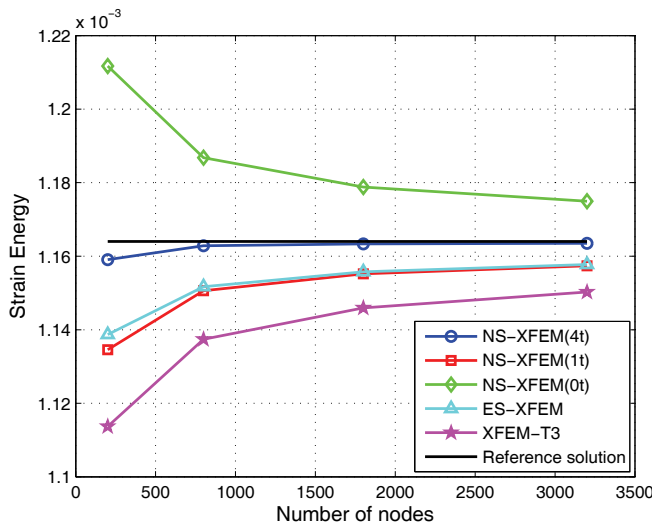
Figure 10: Strain energy for the plate with edge crack under tension

- NS-XFEM(4t) with Heaviside enrichment and tip enrichment Φ, Eq. (12).

- NS-XFEM(1t) with Heaviside enrichment and branch enrichment $\Phi = \sqrt{r} \sin \frac{\theta}{2}$ (the last three terms in Eq. (12) are omitted Rabczuk and Zi (2007)).

- NS-XFEM(0t) with only Heaviside enrichment but without branch tip enrichment.

The results of the NS-XFEM are compared with those of the ES-XFEM [Liu, Chen, Nguyen-Thoi, Zeng, and Zhang (2010)] and the XFEM-T3 (the "standard" XFEM
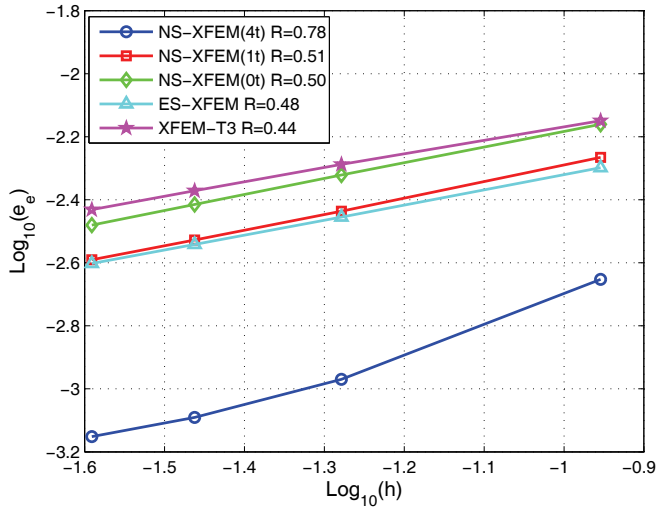
Figure 11: The convergence in the energy norm vs. *h* (mesh size) for the plate with edge crack under tension
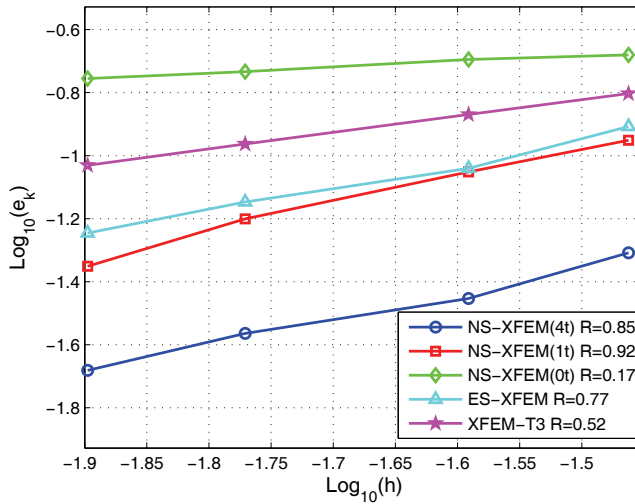
Figure 12: The convergence in the stress intensity factor K_I vs. *h* (mesh size) for the plate with edge crack under tension

formulation) with full tip enrichment. Both, ES-XFEM and XFEM-T3, employ the Heaviside enrichment and the full tip enrichment of Eq. (12). Figure 10 shows that the strain energy of NS-XFEM(4t) and NS-XFEM(1t) models is closer to the reference value compared to the ES-XFEM. The NS-XFEM(0t) results in an upper-bound solution. We note that the tip enriched NS-XFEM formulations does not result in an upper bound solution. The convergence rates in terms of the strain energy norm and SIF K_I for different numerical methods are depicted in Figure 11 and Figure 12. The NS-XFEM (4t) achieves super-convergent results and is more accurate than both ES-XFEM and XFEM-T3. The NS-XFEM (1t) almost produces the same results as the ES-XFEM.

4.2 Plate with edge-crack under shear
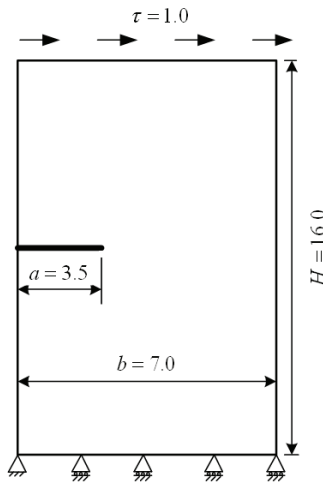
Figure 13: Plate with edge crack under shear

In this example, we consider the edge crack geometry subjected to a shear load as shown in Figure 13. The material parameters are Young's modulus $E = 3 \times 10^7 Pa$ and Poisson's ratio $v = 0.25$. The exact stress intensity factors for this load case are given [Yau, Wang, and Corten (1980)] by

$$K_I = 34.0 Pa\sqrt{mm}; K_{II} = 4.55 Pa\sqrt{mm} \tag{27}$$
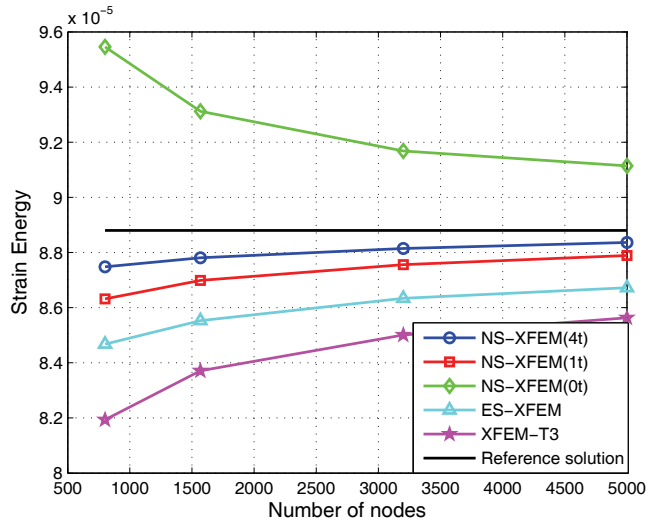
Figure 14: Strain energy for plate with edge crack under shear
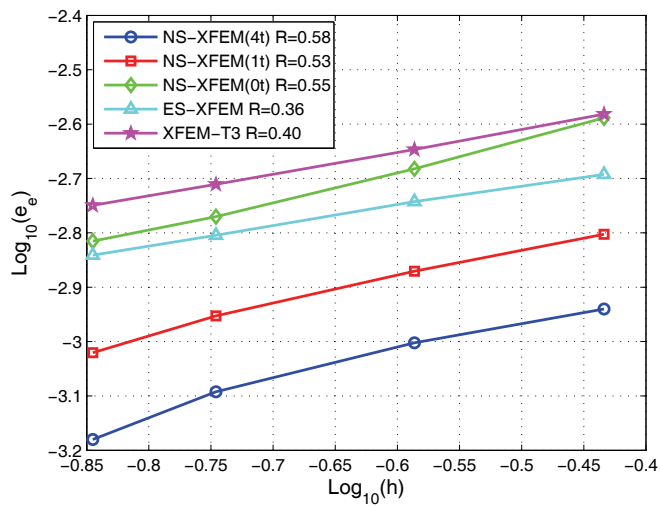
Figure 15: The convergence in the energy norm vs. *h* (mesh size) for plate with edge crack under shear
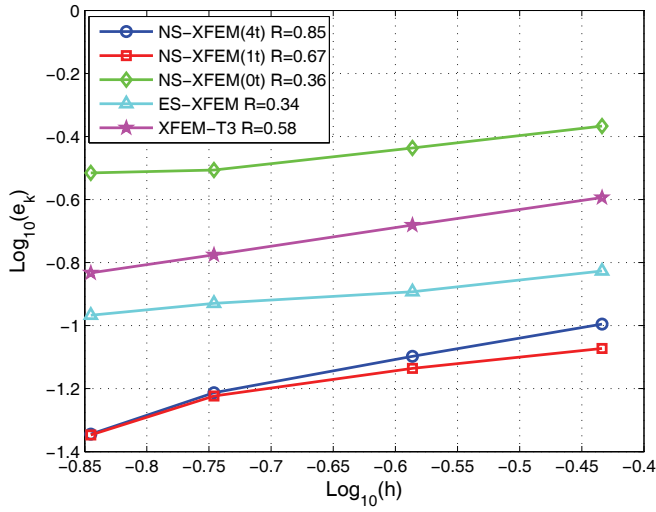
Figure 16: The convergence in the stress intensity factor K_I vs. h (mesh size) for plate with edge crack under shear
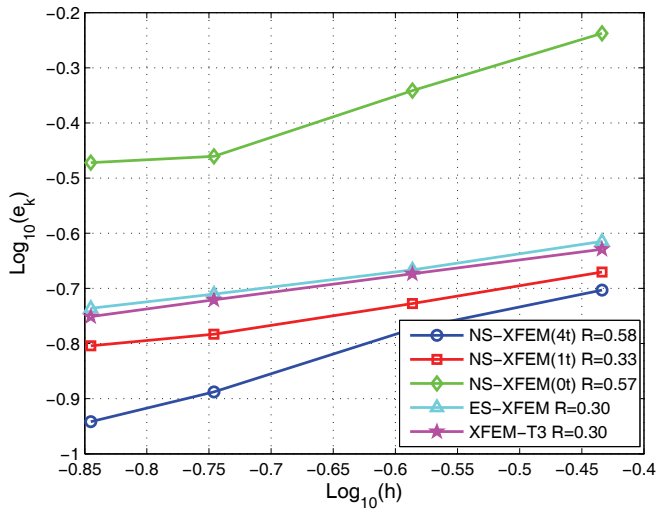
Figure 17: The convergence in the stress intensity factor K_{II} vs. h (mesh size) for plate with edge crack under shear

The results from Figure 14 to Figure 17 show that the NS-XFEM (1t) and NS-XFEM (4t) results are more accurate than those of ES-XFEM and XFEM-T3. NS-XFEM(4t) maintains superconvergent solutions and the NS-XFEM(0t) produces an upper bound solution in the strain energy.

5   Conclusions

We presented a novel numerical method called NS-XFEM that combines NS-FEM and XFEM for analysis of two-dimensional linear elastic fracture problems. Some benchmarks examples were performed and we computed the convergence rate in terms of strain energy and stress intensity factor. The results of NS-XFEM were then compared to those of ES-XFEM and the standard XFEM-T3. It was shown that the NS-XFEM can produce superconvergent solutions. The present method also simplifies the integration of discontinuous approximation by transforming interior integration into boundary integration. More importantly, no derivatives of shape functions are needed to compute the stiffness matrix. As a result, the integration of singular functions is avoided when the Westergaard solution is inserted into the approximation.

Future applications of NS-XFEM may include complex problem such as the failure of concrete under large deformations, multiple crack initiation and propagation [Rabczuk, Zi, Bordas, and Nguyen-Xuan (2008)] and branching in 3D [Rabczuk and Bordas (2007); Bordas, Rabczuk, and Zi (2008)].This will be studied in the future.

References

Belytschko, T.; Black, T. (1999):   Elastic crack growth in finite elements with minimal remeshing. *International Journal for Numerical Methods in Engineering*, vol. 45, pp. 602–620.

Bordas, S.; Natarajan, S. (2010):   On the approximation in the smoothed finite element method (sfem). *International Journal for Numerical Methods in Engineering*, vol. 81, pp. 660–670.

Bordas, S.; Rabczuk, T.; Nguyen-Xuan, H.; Nguyen-Vinh, P.; Natarajan, S.; Bog, T.; Do-Minh, Q.; Nguyen-Vinh, H. (2008):   Strain smooth-

ing in FEM and XFEM. *Computers and Structures*, vol. in press, pp. doi:10.1016/j.compstruc.2008.07.006.

Bordas, S.; Rabczuk, T.; Zi, G. (2008): Three-dimensional crack initiation, propagation, branching and junction in non-linear materials by an extended mesh-free method without asymptotic enrichment. *Engineering Fracture Mechanics*, vol. 75(5):, pp. 943–60.

Canh, V. L.; Nguyen-Xuan, H.; Askes, H., B. S.; Rabczuk, T.; Nguyen-Vinh, H. (2010): A cell based smoothed finite element method for kinematic limit analysis. *International Journal for Numerical Methods in Engineering*, vol. 46, pp. 679–701.

Chen, J. S.; Wu, C. T.; Yoon, S.; You, Y. (2000): A stabilized conforming nodal integration for galerkin meshfree method. *International Journal for Numerical Methods in Engineering*, vol. 50, pp. 435–466.

Chen, L.; Rabczuk, T.; Liu, G. R.; Zeng, K. Y.; Kerfriden, P.; Bordas, S. (2010): Extended finite element method with edge-based strain smoothing (esm-xfem) for linear elastic crack growth. *International Journal for Numerical Methods in Engineering*, vol. accepted.

Dai, K. Y.; Liu, G. R.; Nguyen, T. T. (2007a): An n-sided polygonal smoothed finite element method (nSFEM) for solid mechanics. *Finite elements in analysis and design*, vol. 43, pp. 847–860.

Laborde, P.; Pommier, J.; Renard, Y.; Salaun, M. (2005): High-order extended finite element method for cracked domains. *International Journal for Numerical Methods in Engineering*, vol. 64, pp. 354–381.

Li, F.; Shih, C.; Needleman, A. (1985): A comparison of methods for calculating energy rates. *Engineering Fracture Mechanics*, vol. 21(2), pp. 405–421.

Liu, G.; Nguyen, T.; Dai, K.; Lam, K. (2007): Theoretical aspects of the smoothed finite element method (SFEM). *International Journal for Numerical Methods in Engineering*, vol. 71, pp. 902–930.

Liu, G.; Nguyen-Thoi, T.; Nguyen-Xuan, H.; Lam, K. (2009): A node-based smoothed finite element method (NS-FEM) for upper bound solutions to solid mechanics problems. *Computers and Structures*, vol. 87, pp. 14–26.

Liu, G. R.; Chen, L.; Nguyen-Thoi, T.; Zeng, K. Y.; Zhang, G. Y. (2010): A novel singular node-based smoothed finite element method (ns-fem) for upper bound solutions of fracture problems. *International Journal for Numerical Methods in Engineering*, vol. 83, pp. 1466–1497.

Liu, G. R.; Dai, K. Y.; Nguyen, T. T. (2007): A smoothed element method for mechanics problems. *Computational Mechanics*, vol. 39, pp. 859–877.

Liu, G. R.; Nguyen-Thoi, T.; Lam, K. Y. (2009): An edge-based smoothed finite element method (ES-FEM) for static, free and forced vibration analyses of solids. *Journal Sound and Vibration*, vol. 320, pp. 1100?1130.

Melenk, J.; Babuška, I. (1997): The partition of unity finite element method: basic theory and applications. *CMAME*, vol. 40, pp. 727–758.

Moes, N.; Dolbow, J.; Belytschko, T. (1999): A finite element method for crack growth without remeshing. *International Journal for Numerical Methods in Engineering*, vol. 46, pp. 131–150.

Moran, B.; Shih, C. (1987): Crack tip and associated domain integrals from momentum and energy balance. *Engineering Fracture Mechanics*, vol. 27(6), pp. 615–641.

Nguyen-Thanh, N.; Rabczuk, T.; Nguyen-Xuan, H.; Bordas, S. (2008): A smoothed finite element method for shell analysis. *Computer Methods in Applied Mechanics and Engineering*, vol. 198, pp. 165–177.

Nguyen-Thanh, N.; Rabczuk, T.; Nguyen-Xuan, H.; Bordas, S. (2009): An alternative alpha finite element method with discrete shear gap technique for analysis of mindlin-reissner plates. *Finite Elements in Analysis and Design*, vol. in Proof.

Nguyen-Thanh, N.; Rabczuk, T.; Nguyen-Xuan, H.; Bordas, S. (2010): An alternative alpha finite element method (a"fem) free and forced vibration analysis of solids using triangular meshes. *Journal of Computational and Applied Mathematics*, vol. 233(9), pp. 2112–2135.

Nguyen-Thoi, T.; Liu, G. R.; Lam, K. Y.; Zhang, G. Y. (2009): A face-based smoothed finite element method (FS-FEM) for 3d linear and nonlinear solid mechanics problems using 4-node tetrahedral elements. *International Journal for Numerical Methods in Engineering*, vol. 78, pp. 324–353.

Nguyen-Thoi, T.; Vu-Do, H.; Rabczuk, T.; Nguyen-Xuan, H. (2010): A node-based smoothed finite element method (ns-fem) for upper bound solution to visco-elastoplastic analysis of solids using triangular and tetrahedral meshes. *Computer Methods in Applied Mechanics and Engineering*, vol. 199, pp. 3005–3027.

Nguyen-Xuan, H.; Bordas, S.; Nguyen-Dang, H. (2008): Smooth finite element methods: Convergence, accuracy and properties. *International Journal for Numerical Methods in Engineering*, vol. 74, pp. 175–208.

Nguyen-Xuan, H.; Rabczuk, T.; Nguyen-Thanh, N.; Nguyen-Thoi, T.; Bordas, S. (2010): A node-based smoothed finite element method with stabilized discrete shear gap technique for analysis of reissner?mindlin plates. *Computational Mechanics*, vol. 46, pp. 679–701.

Rabczuk, T.; Areias, P. (2006): A meshfree thin shell for arbitrary evolving cracks based on an external enrichment. *Computer Modeling in Engineering and Sciences*, vol. 16, no. 2, pp. 115–130.

Rabczuk, T.; Belytschko, T. (2004): Cracking particles: A simplified mesh-free method for arbitrary evolving cracks. *International Journal for Numerical Methods in Engineering*, vol. 61, no. 13, pp. 2316–2343.

Rabczuk, T.; Belytschko, T. (2007): A three dimensional large deformation meshfree method for arbitrary evolving cracks. *Computer Methods in Applied Mechanics and Engineering*, vol. 196, no. 29-30, pp. 2777–2799.

Rabczuk, T.; Bordas, S.and Zi, G. (2007): A three dimensional meshfree method for static and dynamic multiple crack nucleation/propagation with crack path continuity. *Computational Mechanics*, vol. 40, no. 3, pp. 473–495.

Rabczuk, T.; Eilb, J. (2006): Modelling dynamic failure of concrete with mesh-free methods. *International Journal for Impact Engineering*, vol. 32, no. 2, pp. 1878–1897.

Rabczuk, T.; Samaniego, E. (2008): Discontinuous modelling of shear bands with adaptive meshfree method. *Computer Methods in Applied Mechanics and Engineering*, vol. 197, no. 6-8, pp. 641–658.

Rabczuk, T.; Wall, W. A. (2006): Extended finite element and meshfree methods. *Technical University of Munich, Germany*, vol. WS200/2007.

Rabczuk, T.; Zi, G. (2007): A meshfree method based on the local partition of unity for cohesive cracks. *Computational Mechanics*, vol. 39, no. 6, pp. 743–760.

Rabczuk, T.; Zi, G.; Bordas, S.; Nguyen-Xuan, H. (2008): A geometrically nonlinear three dimensional cohesive crack method for reinforced concrete structures. *Engineering Fracture Mechanics*, vol. 75(16), pp. 4740–58. doi:10.1016/j.engfracmech.2008.06.019.

Strouboulis, J. T.; Babuška, I.; Copps, K. (2000): The design and analysis of the generalized finite element method. *Computer Methods in Applied Mechanics and Engineering*, vol. 181, pp. 43–96.

Yau, J. F.; Wang, S. S.; Corten, H. T. (1980): A mixed-mode crack analysis of rectilinear anisotropic solids using conservation laws of elasticity. *International Journal of Fracture*, vol. 16(3), pp. 247–59.